

## Acoustic Measurement of Bubble Size Distributions: Theory & Experiments

Sankar Prabhukumar, Ramani Duraiswami, Georges L. Chahine  
DYNAFLOW, Inc., 7210 Pindell School Road, Fulton, MD 20759

### INTRODUCTION

Determination of bubble populations in a sample of liquid is important in many fields. Among the methods used, a successful acoustic method has advantages in that bubbles are very responsive to sound, that reasonably large volumes may be sampled, and that the method can be relatively inexpensive.

While previous investigators had used approximate solution techniques, we used in Duraiswami (1993) consistent equations for sound propagation in liquids derived by Prosperetti et al (1989), and developed a method for solving the ill-posed equations relating the acoustic measurements to the bubble population density directly. A constrained minimization approach coupled with a regularization strategy that renders these equations well-posed was employed.

In the present work we test the developed method and algorithms on analytical data first, and find that the methods are successful in recovering the bubble density function, and perform much better than previous solution techniques. Next we perform experiments to measure bubble populations using the developed method. The bubbles are generated artificially using electrolysis and air injection through porous tubes. The predicted results for the bubble population are compared to those obtained by microphotography. The results obtained indicate that the method provides accurate measurements of the bubble population. Based on these results an instrument, the Acoustic Bubble Spectrometer (ABS), is being developed.

### GOVERNING EQUATIONS

An acoustic dispersion relation for a *given bubble population* in a bubbly fluid was developed by Commander and Prosperetti, 1989. In the present study we reverse the process and use this equation to *deduce* the bubble population from *given measurements*

of sound attenuation and change in phase velocity.

Using the dispersion relation we arrive at two Fredholm integral equations of the first kind which relate the bubble density function  $N(a)$  to sound speed ratio  $u$  and attenuation factor  $v$  defined as follows:

$$u(f) = \frac{c_l}{c_m}, \quad v(f) = -\frac{c_l}{4\pi f d} \log \left( \frac{\bar{p}^2}{\bar{p}_{ref}^2} \right) \quad (1)$$

where  $f$  is the frequency of insonification;  $c_l$  is the speed of sound in pure liquid while  $c_m(f)$  is that in the bubbly medium;  $\bar{p}_{ref}^2(f)$  is the Mean Square Amplitude (MSA) of the pressure signal at a distance  $d$  from the source in pure water, and  $\bar{p}^2(f)$  is the corresponding quantity in the bubbly medium. These quantities are particularly suited for experimental measurements as the data have already been shown to be *very sensitive to the bubble size distribution*. The governing equations are given by:

$$\int_{a_{lo}}^{a_{hi}} k_1(f, a) N(a) da - u^2 - v^2 - 1 = \alpha_1(f), \quad (2)$$

$$\int_{a_{lo}}^{a_{hi}} k_2(f, a) N(a) da = uv = \alpha_2(f). \quad (3)$$

Here  $a$  is the bubble radius,  $a_{lo}$  and  $a_{hi}$  are the minimum and maximum bubble radii expected;  $k_1$  and  $k_2$  are the following kernel functions:

$$k_1(f, a) = 4\pi \left( \frac{c_l}{f} \right)^2 \frac{a \left( (f_0/f)^2 - 1 \right)}{\left( (f_0/f)^2 - 1 \right)^2 + 4\delta^2}, \quad (4)$$

$$k_2(f, a) = 4\pi \left( \frac{c_l}{f} \right)^2 \frac{a\delta}{\left( (f_0/f)^2 - 1 \right)^2 + 4\delta^2}, \quad (5)$$

where  $f_0$  and  $\delta$  are respectively the resonant frequency and damping constant of a bubble of radius  $a$ , at anisonifying frequency  $f$ . The details of the derivation, and the numerical calculation of the kernel functions can be found in Duraiswami and Chahine (1992).

## SOLUTION METHOD

The equations (2) and (3) cannot be solved analytically. Previous investigators had used a low volume fraction simplification of equation (3) to obtain the bubble population (see Wildt 1949, Sarkar and Prosperetti 1994). The resulting integral equation was solved using approximate techniques (Wildt 1949, Vagle and Farmer, 1992). These approximate methods have been shown to lead to significant errors by Commander and Moritz, 1989. However, if one attempts an accurate numerical solution of the equations one faces the problem that the equations are ill-posed. It is, therefore, necessary to look for the solution of a stable approximate problem, which in some sense is the closest to the chosen exact solution. This process is termed *regularizing* the problem. This is achieved by imposing *a priori* constraints on the solution. In a physical problem the solution is known to satisfy certain constraints. Imposition of these constraints explicitly restricts the solution set, and can restore uniqueness and/or well-posedness to the problem.

We studied a number of different methods for solving the inverse problem and found that the following novel technique, based on linear optimization, was best (Duraiswami, 1993). In this approach we minimize  $|K_2N - \alpha_2|$ , subject to

$$\begin{aligned} K_1N &= \alpha_1, N(a) \geq 0, \int_{a_{i_0}}^{a_{h_i}} N(a)a^2 da < C_1, \\ \text{and } \int_{a_{i_0}}^{a_{h_i}} N(a)a^3 da &< C_2. \end{aligned} \quad (6)$$

where  $K_1$  and  $K_2$  represent the integral operators with kernel functions  $k_1$  and  $k_2$ . Here, the objective function comes from equation (3), and the first constraint comes from the fact that equations (2) and (3) must be simultaneously satisfied.  $C_1$  and  $C_2$  are constants which are larger than the expected surface area per unit volume and the volume fraction of bubbles. The above equations are placed in a linear programming formulation and solved. The use of the constrained optimization formulation allows incorporation of further experimental constraint information in the solution procedure.

## EXPERIMENTAL SET-UP AND PROCEDURE

The objective of the experiments is to measure  $u$  and  $v$  defined in Equations (1). An experiment consists of emitting in the bubbly medium a signal from a hydrophone, at a particular frequency and receiving the signal with a second hydrophone. To avoid interference between the signal directly received and that

reflected from neighboring walls, the duration of emission of the signal  $\tau_e$  is limited as follows:

$$\tau_e < (2d_m - d)/c_l. \quad (7)$$

where  $d_m$  is the distance between the emitting hydrophone and the closest reflecting boundary. The emitter excitation and received signals are acquired using a data acquisition board. The procedure is repeated over a range of frequencies and the recorded signals are then analyzed to obtain  $u$  and  $v$  as functions of frequency. These are then used as input to the inverse problem solver.

In the experiments reported below we used two Brüel and Kjaer model 8103 hydrophones. These are calibrated for sensitivity in both emission and reception over a range of frequencies from 5 kHz to 190 kHz. Monochromatic waves were generated using a Pulse/Function generator which drove one hydrophone. Both output frequency and the duration of the signals generated can be precisely controlled using a multi-purpose data acquisition board. The signals were stored using the same board, which has digital to analog conversion resolution of 12 bits, has programmable gain, and can sample at a maximum rate of  $10^6$  samples per second. With our current set-up we can perform measurements over the interesting range of frequencies within a half second interval. Typically measurements at about 38 frequencies are made. This enables multi-frequency acquisition in a very short period of time (time scale much smaller than time for the bubble population evolution time). When desired, the experiments were repeated a number of times in succession and averaged signals obtained. The experiments were performed in a smaller plexiglas tank of dimensions  $24'' \times 16'' \times 12''$ , or a larger cubical tank with each side of length 6 feet. Figure 1 illustrates the set-up.

**Bubble Generators** Bubble generators were manufactured to generate bubbles of different sizes in water and thereby create a bubbly medium for testing. The bubble generators were located at the bottom of the tank. Three different bubble generation techniques were employed.

*Electrolysis* at stainless steel wires was used to generate small bubbles ( $<200$  microns). Wires of two different sizes were used to generate bubbles of different sizes.

*Compressed air* was pumped through pores in in-house manufactured microporous tubes (DYNAPERM<sup>R</sup>) which produced bubbles of size much larger than those generated using electrolysis ( $\sim 1$ mm radius).

*Electrolysis / compressed air coupled with shear-flow:* Coupling a shear flow with the above generation techniques allows generation of finer bubble sizes.

With electrolysis we can obtain bubbles as small as 20 microns.

**Signal Processing Procedure** Signal processing software was developed to analyze the data acquired during the experiments. The goal of the analysis is to determine, at each frequency, the time taken for the sound packet to traverse the distance between the hydrophones, and the mean-squared amplitude of the received packet.

**Determination of phase velocity:** Since the hydrophone requires a finite amount of time to respond to a sudden change in voltage, and the delay in time between emission and reception is small, the response time could result in large errors in the speed of sound calculated. The effect of this finite response of the hydrophone is removed by deconvolving the received signal with a stored response of the hydrophone system to an impulse function. The time delay  $\Delta T$  between the emitted signal and the *deconvolved* received signals is obtained by cross-correlating the two signals. The location of the peak of the cross-correlation yields  $\Delta T$  from which the sound speed  $c_m$  can be obtained.

**Determination of Attenuation:** The mean square amplitude (MSA) calculation was done both in the time and frequency domains to get two estimates. The reference MSA in Equation (1) is that of the received signal when there are *no injected bubbles*. It can be obtained using either of two methods.

In the first method, using the emitting hydrophone emission calibration curves the reference MSA is obtained assuming spherical wave propagation of the emitted signal. In this case the calibration data provided by the manufacturer are digitized and stored on the computer.

In the second method, the entire set of experiments is first performed in "pure" water (i.e. with no bubbles generated). The MSA in the received signals obtained from these experiments is used as reference. In this approach sources of error that are common to experiments with and without bubbles are eliminated.

## INVERSE PROBLEM SOLUTION

The inverse problem solution is sensitive to the choice of parameters such as the constraints and equations used in the procedure, and to the errors in  $u$  and  $v$  input data. A series of calculations were performed to study the effect of these different parameters on the final bubble distribution, and to optimize the solution procedure before using it on experimental data. A sample result of the procedure is shown in Figures 2 and 3. The inverse problem is solved using input  $u(f)$  and  $v(f)$  data shown in Figure 2 generated from an assumed bubble distribution shown as a continuous line in Figure 3.

## Sensitivity of inverse problem to errors in $u$ and $v$

A comprehensive study of the effect of errors in the generated  $u$  and  $v$  input data on the calculated bubble distribution was performed using the  $u$  and  $v$  data calculated from the forward problem. Systematic and random errors were introduced in  $u$  and  $v$  data and the effect of these errors on the bubble distribution estimate was studied. The noisy input data were generated from the original curves by introducing a maximum error of 5% in the  $u$  and 50% in the  $v$  data. Figure 4 shows the original and noisy  $u$  and  $v$  curves. Figure 5 compares the computed bubble distribution using the erroneous values with the original assumed distribution. The figure clearly illustrates the tolerance of the inverse problem solution to errors in data.

## Comparison of inverse problem solution methods

The ABS inverse solution results were also compared with other existing acoustic procedures.

*Wildt:* Wildt (1949) derived the following expression for the bubble size distribution  $N(a)$ :

$$N(a_R) = 4f^2v/(c^2a_R^2), \quad (8)$$

where  $a_R$  is the resonant radius corresponding to the insonification frequency.

*Vagle-Farmer:* Vagle and Farmer (1992) modified the above Wildt procedure and approximated the integral equation involving  $k_2$  as follows:

$$\int_0^\infty k_2(a, f)N(a)da \simeq 2N(a_R) \int_0^{a_R} k_2(a, f)da. \quad (9)$$

They only assumed that  $N(a)$  could be extracted out from under the integral sign and then approximated the remaining integral by twice the value of the integral from 0 to  $a_R$ .

The bubble distributions from these two methods are compared with that of the inverse problem solution in Figure 6. The dotted line in the figure represents the original assumed distribution. The continuous line with circles shows our solution, with squares shows the Wildt solution, and with triangles shows the Vagle-Farmer solution. The figure shows that the Wildt and Vagle-Farmer solutions fail to produce reasonable estimates for such bubble distributions.

## Solution procedure verification using synthetic data

The signal analysis and inverse problem procedures were verified for consistency using synthetic data generated by assuming a bubble distribution as shown in Figure 7. Using the assumed bubble distribution as a function of radius,  $u$  and  $v$  are obtained by solving the forward problem. The known emitter excitation

voltage signal is convolved with the response of the hydrophone system to a step function. The resulting convolved voltage signal is converted to pressure using the emitter sensitivity curve at the given frequency. Using  $u$ , the time elapsed  $\Delta T$  between the emitter excitation and the synthetic received signal can be obtained knowing the distance  $d$  between the hydrophones. The emitter excitation signal is shifted in time by the calculated  $\Delta T$  and the amplitude of the computed received signal is that of the emitted signal divided by the distance  $d$  (assuming a spherical wave). The resulting pressure signal is converted back to a voltage signal. The voltage  $A_{ref}$  of the resulting signal is that which would be received if there were no bubbles. The additional attenuation due to the bubbles is obtained using the  $v$  value at the given frequency. The new amplitude  $A$  of the signal adjusted for  $v$  is obtained as follows:

$$A = A_{ref} e^{-(2\pi f v r / c_l)}. \quad (10)$$

The above steps are repeated for each frequency under consideration, and the emitter excitation signals and the synthetically generated received signals are used by the signal analysis program to yield back  $u$  and  $v$  curves as functions of frequency. These  $u$  and  $v$  curves are used by the inverse problem program to obtain back the desired bubble distribution curve.

Figure 8 compares the  $u$  and  $v$  curves obtained after performing signal analysis using the synthetic data with the corresponding original curves that were used to generate the data. The figure shows that the back calculated  $u$  curve follows the original  $u$  curve but does not fall exactly on top of the original curve. This small discrepancy can be related to the inaccuracy resulting from the limited sampling frequency of the data acquisition board which has a maximum sampling rate of 1MHz. Figure 7 compares the back calculated bubble distribution shown as a dotted line with the original assumed distribution shown as a continuous line.

## EXPERIMENTAL BUBBLE DISTRIBUTIONS

Experiments were performed using the two B&K hydrophones placed 6 inches apart in the 6 foot cubic tank. Experiments were first performed with no artificial bubbles generated and, they were repeated two hours after starting the bubble generator. In order to minimize noise, each signal was averaged using a set of 20 similar signals.

### Experiments with electrolysis bubbles

Figures 9-11 shows analysis results corresponding to data obtained with bubbles being generated using the electrolysis generator. Figure 9 and 10 shows the  $u(f)$  and  $v(f)$  curves computed at two different times about two hours apart. Figure 11 shows the corresponding bubble distribution curves. The bubble distribution

curves from the inverse problem were grouped by dividing the guesses for minimum and maximum radii  $a_{lo}$  and  $a_{hi}$  into 100 bins. In this case the size of a bin was about 10 microns. It can be seen from the figures that the data are quite repeatable.

**Validation of Results** A preliminary validation of the acoustic results using microphotography was performed. In this preliminary result, the bubbles were not photographed simultaneously with the acoustic measurement. The photographs were of bubbles generated in the smaller plexiglas chamber under identical conditions.

The photographs are scanned in gray-scale format and a threshold level for the gray-scale image is determined based on the closeness of comparison between the thresholded image and the gray-scale image. The thresholded image is then analyzed using developed software to get the area in pixels for each bubble detected. The area of each bubbles is converted to the radius (in meters) of an equivalent circle using the scale. The resulting radii are then grouped into a given number of bins obtained by sub-dividing the maximum and minimum radii of the bubbles. These numbers are then converted to numbers per square meter by dividing the number of bubbles with the area of the scanned image. The resulting data are subsequently extrapolated to numbers per cubic meter by using the depth of field in the photographs taken.

The number density of the bubbles detected using this technique is very sensitive to the threshold level selected. However, the shape of the bubble distribution curve remains more or less the same. Figure 12 compares the resulting bubble distribution computed using ABS with that from image processing. The figure illustrates the close comparison between the two approaches, and thereby validates the ABS solution to a certain extent.

## CONCLUSIONS

The results obtained indicate that the method produces accurate measurements of the bubble population distribution. In ongoing work, we are packaging the method into an user friendly MS-Windows based application that integrates the different components of the system, and produces near real-time estimates of bubble distributions. Efforts are underway to produce instrumentation for bubble detection, void-fraction measurement, and bubble population measurement using the developed techniques.

## ACKNOWLEDEMENTS

This work was supported by the National Science Foundation under grants III-9160484 and III-9301379.

**References**

Commander, K. and Prosperetti, A., 1989. "Pressure waves in bubbly liquids: comparison between theory and experiment," *J. Acoust. Soc. Am.*, **85**, 732-746.

Commander, K. and Moritz, E., 1989. "Off-resonance contributions to acoustical bubble spectra," *J. Acoust. Soc. Am.*, **89**, 592-597.

Duraiswami, R., 1993. "Bubble density measurement using an inverse acoustic scattering technique," *ASME Cavitation and Multiphase Flow Forum*, Washington DC.

Duraiswami, R. and Chahine, G., 1992. "Bubble density measurement using an inverse acoustic scattering technique," DYNFLOW Technical Report 92004-1.

Prosperetti, A., Crum, L., and Commander, K., 1988. "Nonlinear bubble dynamics," *J. Acoust. Soc. Am.*, **83**, 502-513.

Sarkar, K. and Prosperetti, A., 1994. "Coherent and incoherent scattering by oceanic bubbles," *J. Acoust. Soc. Am.*, **96**, 332-341.

Wildt, R., 1949. "Physics of Sound in the Sea, Part IV" *National Research Council*.

Vagle, S., and Farmer, D. 1992. "The measurement of bubble-size distributions by acoustical backscatter," *J. Atmos. Ocean. Tech.*, **9**, 630-644.

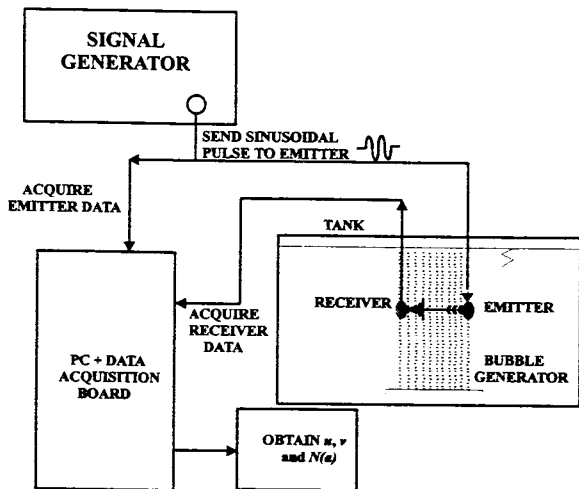


Figure 1: Experimental set-up for bubble counting.

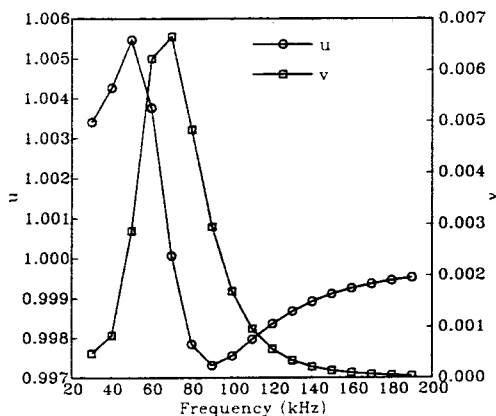


Figure 2:  $u$  and  $v$  curves produced by solving forward problem.

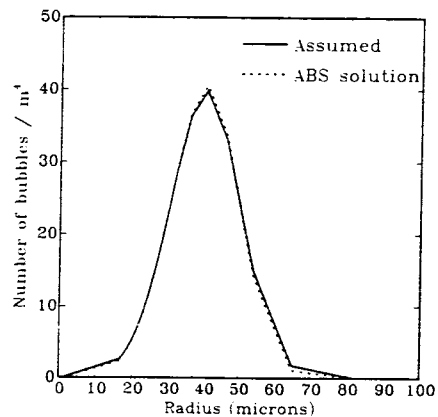


Figure 3: Assumed and calculated bubble distributions.

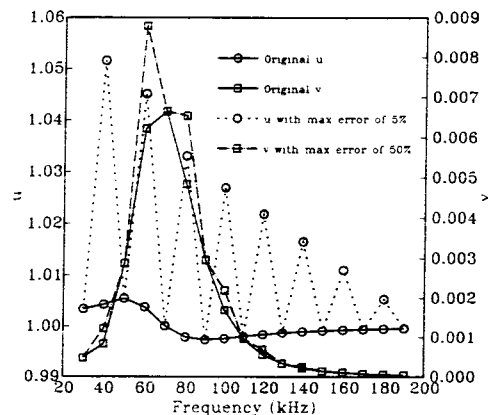


Figure 4: Original and noisy  $u$  and  $v$  curves with a maximum error of 5% in  $u$  and 50% in  $v$ .

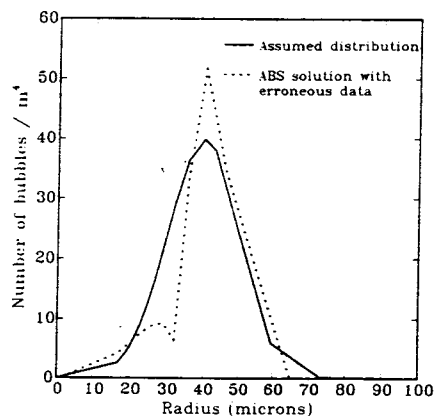


Figure 5: Bubble distribution assumed and calculated using the erroneous data.

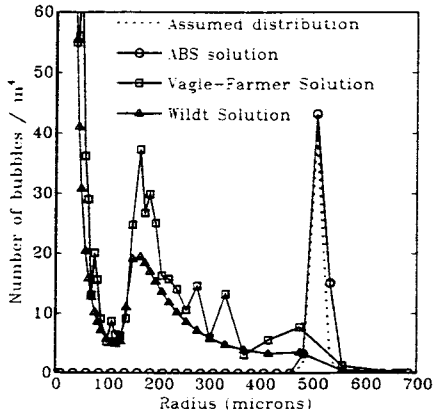


Figure 6: Comparison of ABS, Wildt and Vagle-Farmer solutions, with the assumed bubble distribution.

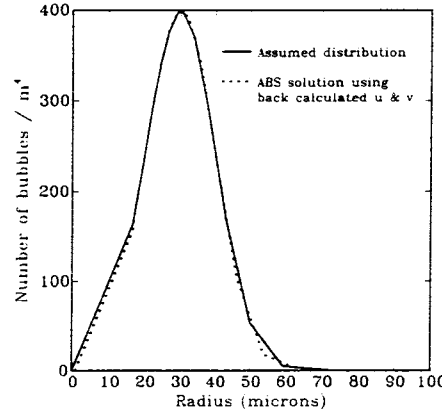


Figure 7: Assumed and back-calculated bubble distributions.

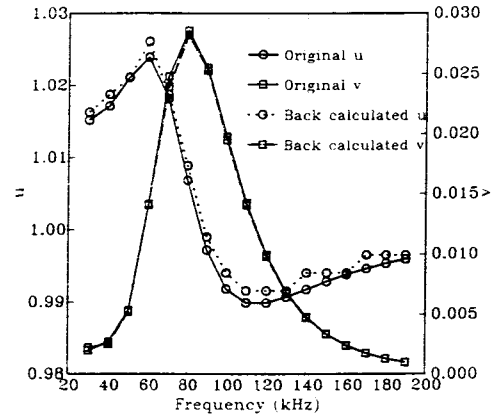


Figure 8: Original and back-calculated u and v curves.

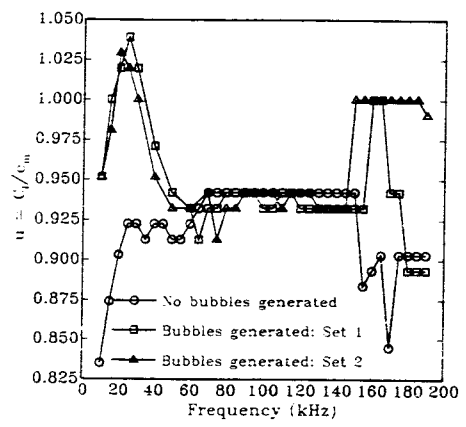


Figure 9:  $u$  calculated from experiments performed with and without bubble generation.

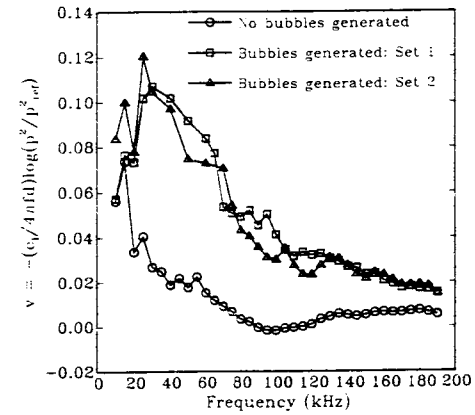


Figure 10:  $v$  calculated using emitter calibration data from experiments performed with and without bubble generation.

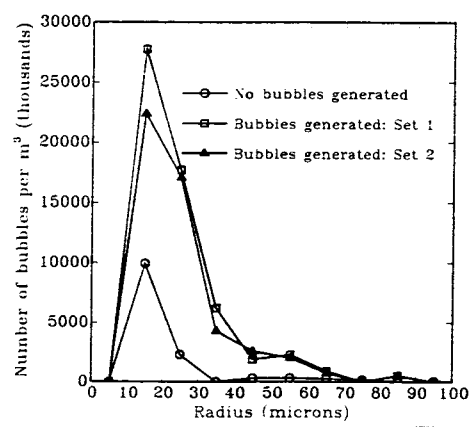


Figure 11: Bubble distribution curves from experiments performed with and without bubble generation.

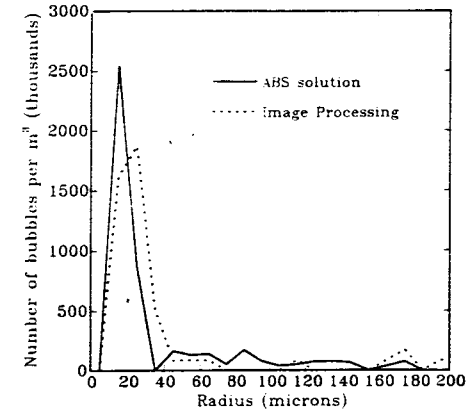


Figure 12: Comparison of results from microphotography and the acoustic technique developed.